Chapter

Wideband Passive and Active Wearable Energy Harvesting Systems for Medical and IOT Applications

Albert Sabban

Abstract

Demand for green energy is in continuous growth in the last years. Compact efficient antennas are crucial for energy harvesting portable systems. Small antennas have low efficiency. The efficiency of communication and energy harvesting systems may be improved by using efficient passive and active antennas. The system dynamic range may be improved by connecting amplifiers to the small antenna feed line. Novel passive and active portable harvesting systems are presented in this chapter. Printed patch, notch and Slot antennas are compact and have low volume. The active antennas may be employed in energy harvesting wearable systems. The antennas and the harvesting system components may be assembled on the same printed board. The printed notch and slot antennas bandwidth are from 40 to 100% for VSWR better than 3:1. The slot antenna gain is around 3 dBi with efficiency higher than 85%. The antennas' electrical parameters were computed in free space and near the human body. The active notch antenna gain is around 23 ± 3dB for frequencies ranging from 200 to 900 MHz. The active notch antenna gain is 13 ± 3 dB for frequencies ranging from 1 to 3 GHz. The active notch and slot antenna noise figure is 0.5 ± 0.3dB for frequencies ranging from 200 MHz to 3 GHz.

Keywords: energy harvesting systems, wearable sensors, active systems, medical applications, sensor chargers

1. Introduction

In the last decade, the idea of employing free space energy in the forms of heat, light, vibration, electromagnetic waves, muscle motion, and other types of energy has become useful and attractive. A number of methods to produce electricity from these different types of energy sources have been developed [1–3]. Energy harvesting systems may eliminate the need to replace batteries everyday and the usage of power cords. In order to use as much free space energy as possible, it is important to collect the electromagnetic power from several wireless communication systems. In these cases, we should use wideband or multiband antennas. The energy harvesting antenna must satisfy several specific requirements related to the system application. Due to considerably low-power densities, highly efficient

radiators are crucial. The antennas should operate at a specific frequency range and polarization. The antenna radiation pattern should have a wide beam width or omnidirectional radiation pattern. Several printed antennas were employed for harvesting energy applications [4–6]. Patch and slot antennas are widely used in communication and medical system [7–24]. Wideband compact slot and notch antennas are good choice to function in wearable harvesting energy systems. Slot and notch antennas are compact and flexible and have low production cost. Moreover, a compact low-cost feed network may be achieved by integrating the amplifiers with the antennas on the same substrate. Printed wearable antennas are widely presented in the literature in the last decade as referred in [7–26]. The human body effect on the electrical performance of wearable antennas at microwave frequencies is not always presented in the literature. Electrical properties of human tissues have been investigated in several papers such as [27, 28]. Several wearable antennas have been presented in papers in the last decade as referred in [22, 28–36]. Wearable printed notch and slot antennas for harvesting energy applications are rarely presented in the literature. A new class of wideband passive and active wearable antennas for harvesting energy applications is presented in this chapter. The system efficiency and dynamic range may be improved by connecting amplifiers to the antenna feed line. The active antenna gain is around 23 dB, and the active antenna noise figure is 0.3 dB for frequencies from 200 to 600 MHz.

2. Energy harvesting systems

In RF energy harvesting systems, electromagnetic waves propagating in free space are captured, stored, and used to charge batteries and for other applications. There is a significant increase in the amount of electromagnetic energy in the air. The expected amount of radio wave in the air in 2013 was 1.5 exabytes per month. However, the expected amount of radio wave in the air in 2017 was 11 exabytes per month (see **Table 1**). Today we can do more computations per kWh as listed in **Table 2**. Energy sources used in harvesting systems are listed in **Table 3**. Wireless communication systems operate in the frequencies from 700 to 2700 MHz. Medical systems operate in the frequencies from 200 to 1200 MHz. WLAN systems operate in the frequencies from 5400 to 5900 MHz.

RF energy is inversely proportional to distance and therefore drops as the distance from a source is increased. Harvested power from RF energy sources is around 0.1 $\mu W/cm^2$. Harvested power from RF energy sources in malls and stadiums may increase to around 1 mW/cm^2. RF energy harvesting concept is shown in **Figure 1**.

The RF energy harvesting system consists of an antenna, a rectifying circuit, and a rechargeable battery. The harvesting energy system operates as a dual mode energy harvesting system. The low-noise amplifier is part of the receiving system. The LNA DC bias voltages are supplied by the receiving system. We can calculate the energy harvesting link budget by using Eqs. (1–4):

Year	Amount of radio wave in free space exabytes per month
2014	2.6
2015	4.4
2016	7
2017	11

Table 1.
Amount of radio wave in free space.

Year	Computations per kWh (1E+09)
1983	10
1985	50
1987	100
1992	1000
1997	10,000
2003	100,000
2008	1,000,000
2010	15,000,000

Table 2.
Computations per kWh.

Energy source	Type	Efficiency	Estimated Harvested Power
Light	Outdoor/indoor	10–25%	100 mW/cm^2
Thermal	Human Industrial	~0.1% ~3%	60 μW/cm^2 ~1–10 mW/cm^2
Vibration	~Hz—human ~kHz—machines	20–50%	~4 μW/cm^3 ~800 μW/cm^3
Electromagnetic	900–2700 MHz Wi-Fi, WLAN	~50%	0.1 μW/cm^2 0.001 μW/cm^2

Table 3.
Energy sources used in harvesting systems.

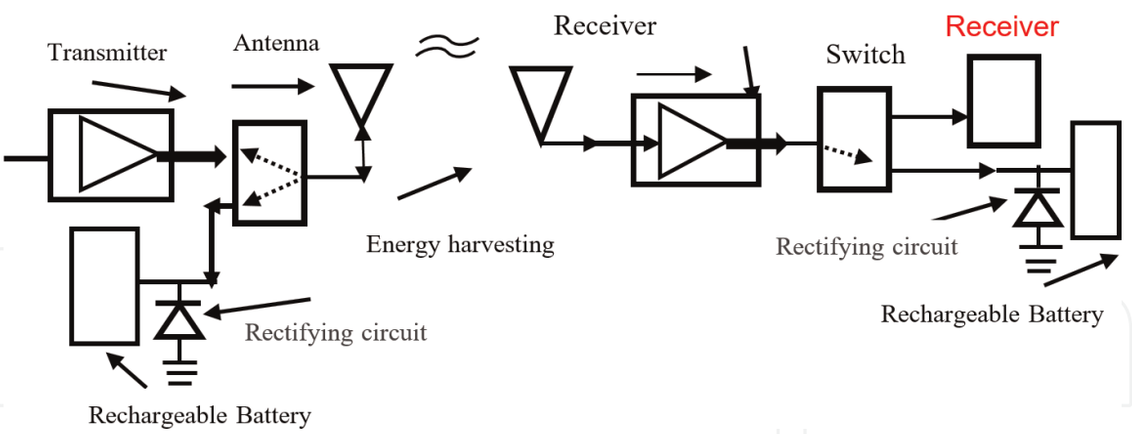

Figure 1.
Dual mode energy harvesting concept.

$$P_r = P_t G_t G_r \left(\frac{\lambda}{4\pi R}\right)^2 \tag{1}$$

Free-space loss (Lp) represents propagation loss in free space. Losses due to attenuation in atmosphere, La, should also be accounted for in the transmission equation, where, $L_p = \left(\frac{4\pi R}{\lambda}\right)^2 \cdot$ The received power may be given as $P_r = \frac{P_t G_t G_r}{L_p}$.

Losses due to polarization mismatch, L_{pol}, should also be accounted. Losses associate with receiving antenna, L_{ra}, and with the receiver, L_r, cannot be neglected in

computation of transmission budget. Losses associate with the transmitting antenna as written as L_{ta}.

$$P_r = \frac{P_t G_t G_r}{L_p L_a L_{ta} L_{ra} L_{pol} L_o L_r} \tag{2}$$

$P_t = P_{out}/L_t$, EIRP = $P_t G_t$.

where P_t = transmitting antenna power; L_t = loss between the power source and antenna; EIRP = effective isotropic radiated power.

$$\begin{aligned} P_r &= \frac{P_t G_t G_r}{L_p L_a L_{ta} L_{ra} L_{pol} L_{other} L_r} \\ &= \frac{EIRP \times G_r}{L_p L_a L_{ta} L_{ra} L_{pol} L_{other} L_r} \\ &= \frac{P_{out} G_t G_r}{L_t L_p L_a L_{ta} L_{ra} L_{pol} L_{other} L_r} \end{aligned} \tag{3}$$

where $G = 10 \cdot \log\left(\frac{P_{out}}{P_{in}}\right)$ dB gain in dB; $L = 10 \cdot \log\left(\frac{P_{in}}{P_{out}}\right)$ dB loss in dB.

The received power P_r in dBm is given in Eq. (4). The received power P_r is commonly referred to as "Carrier Power."

$$P_r = EIRP - L_{ta} - L_p - L_a - L_{pol} - L_{ra} - L_{other} + G_r - L_r \tag{4}$$

Wireless smart phone using standard 802.11 can transmit up to 1 W.
PCMCIA cards using standard 802.11 can transmit around 10 mW up to 100 mW.

3. Wideband notch antenna, 2–7.8 GHz, for energy harvesting applications

A compact notch antenna was printed on a dielectric substrate with dielectric constant of 2.2. The antenna dimensions are 116.4 × 71.4 × 1.2 mm, as presented in **Figure 2**. The antenna bandwidth for VSWR better than 2.5:1 is around 90–100% (see **Figure 3**). The notch antenna has VSWR better than 3:1 at frequencies from 2.1

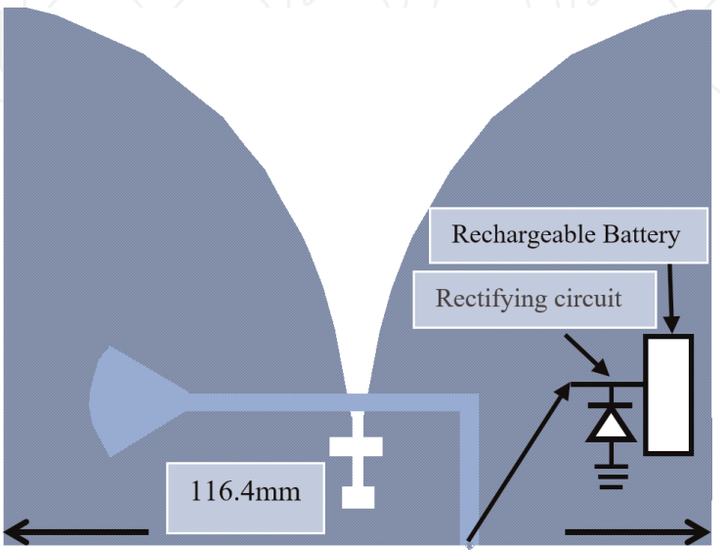

Figure 2.
A wideband 2–7.8 GHz energy harvesting notch.

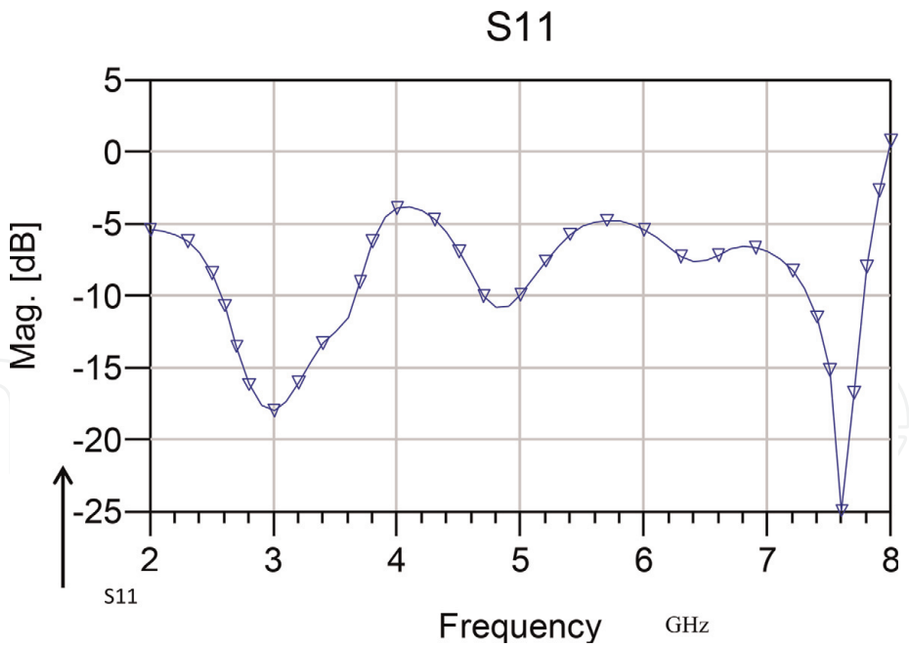

Figure 3.
A wideband 2–7.8 GHz notch, computed S11.

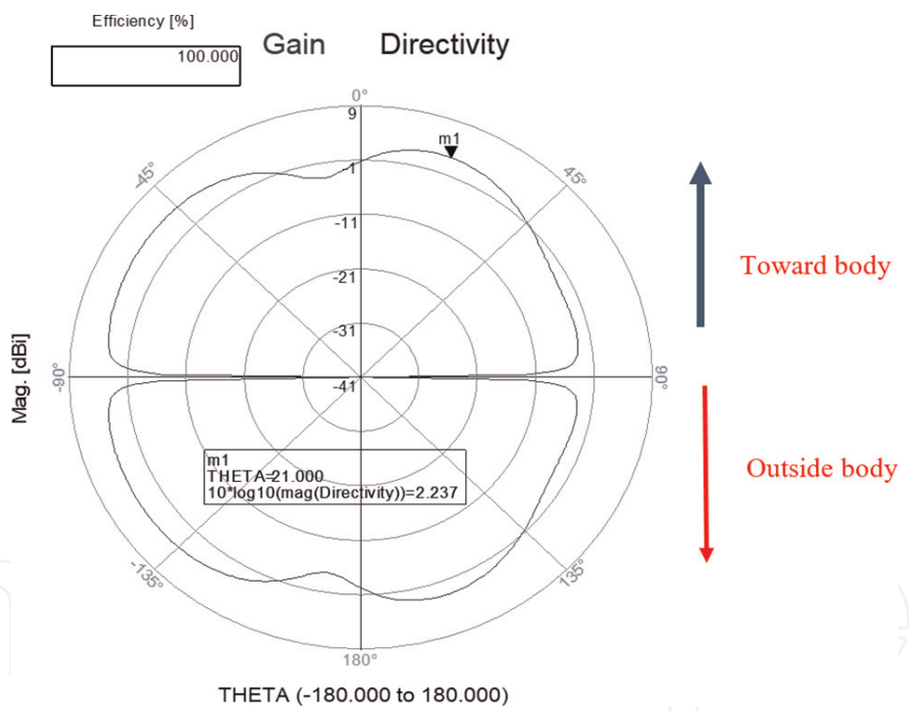

Figure 4.
Radiation pattern of the notch antenna at 3.5 GHz.

to 7.8 GHz. The antenna beam width is around 80° at 5 GHz. The antenna gain is around 2.5 dBi at 3 GHz. The notch antenna radiation pattern at 3.5 GHz is presented in **Figure 4**. The electromagnetic energy is converted to DC energy by a rectifying circuit connected to the antenna input. A rechargeable battery is connected to the output of the rectifying circuit.

4. New wideband active 0.5–3 GHz energy harvesting notch antenna

Harvested power from RF transmitting links is usually lower than 0.1 μW/cm^2. Active antennas may improve the energy.

Improve harvesting system efficiency. A wideband active notch antenna with fractal structure was printed on a 1.2 mm thick with dielectric constant of 2.2. The compact active notch antenna is shown in **Figure 5**. The notch antenna dimensions are 74.5 × 57.1 mm. The antenna center frequency is 1.75 GHz. The active antenna bandwidth is around 150–200% for VSWR better than 3:1. The notch antenna gain, S21 parameter, is presented in **Figure 6**. The active antenna gain is 23 ± 3 dB for frequencies from 200 to 900 MHz.

The active notch antenna VSWR is better than 3:1 for frequencies from 0.5 to 3 GHz. The antenna beam width is around 84° at 1 GHz. A compact E-PHEMT LNA, low-noise amplifier, is connected to the notch antenna via an input matching network. An output matching network connects the amplifier port to the rectifying circuit. A printed compact DC voltage bias network supplies the bias voltages to the harvesting system. The amplifier specification is listed in **Table 4**. The amplifier

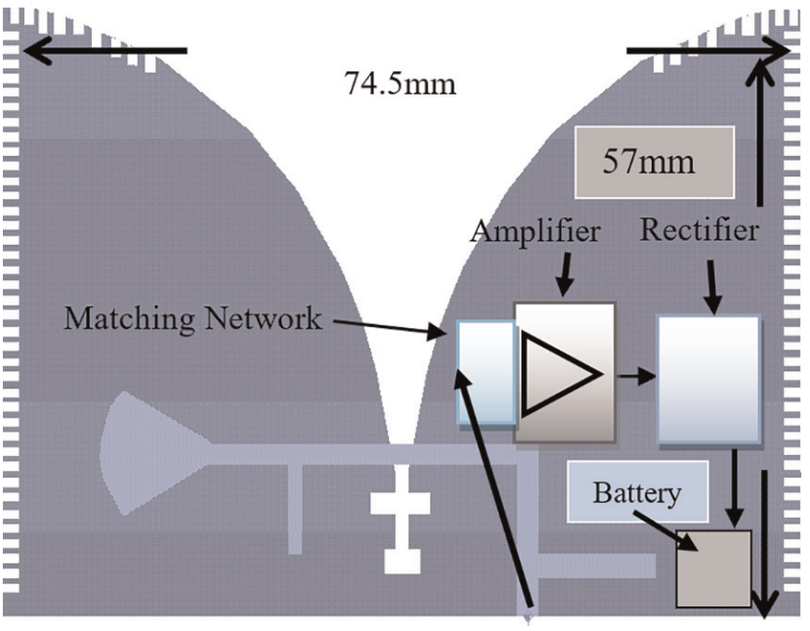

Figure 5.
A wideband fractal active notch antenna.

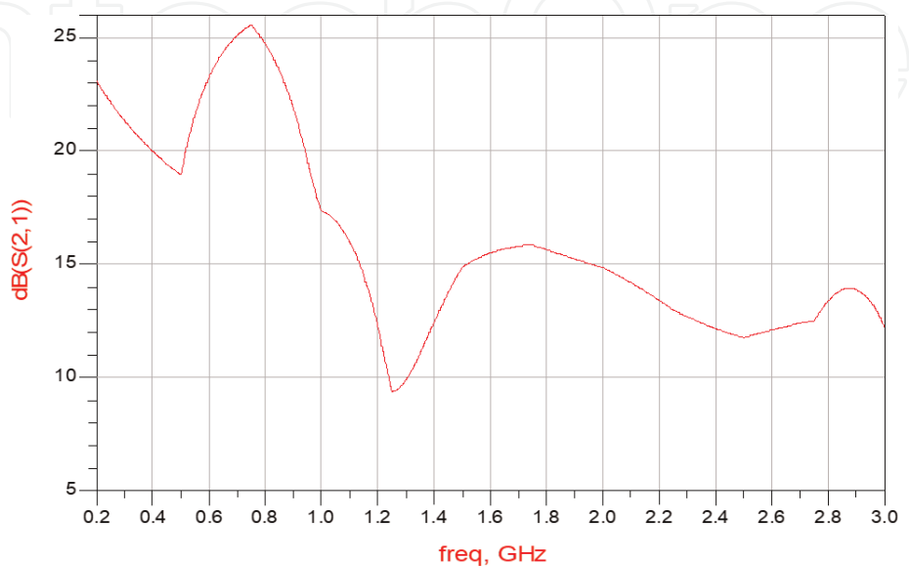

Figure 6.
Active notch antenna S21 parameter.

Parameter	Specification	Remarks
Frequency range	0.4–3 GHz	
Gain	26 dB at 0.4 GHz 18 dB at 2 GHz	Vds = 3 V; Ids = 60 mA
Noise figure	0.4 dB at 0.4 GHz 0.5 dB at 2 GHz	Vds = 3 V; Ids = 60 mA
P1dB	18.9 dBm at 0.4 GHz 19.1 dBm at 2 GHz	Vds = 3 V; Ids = 60 mA
OIP3	32.1 dBm at 0.4 GHz 33.6 dBm at 2 GHz	Vds = 3 V; Ids = 60 mA
Max. input power	17 dBm	
Vgs	0.48 V	Vds = 3 V; Ids = 60 mA
Vds	3 V	
Ids	60 mA	
Supply voltage	±5 V	
Operating temp.	−40–80°C	

Table 4.
LNA amplifier specification.

complex S parameters are listed in **Tables 5** and **6**. The amplifier noise parameters are listed in **Table 7**.

The active antenna gain is 12 ± 3 dB for frequencies from 1 to 3 GHz. The active notch antenna noise figure is 0.5 ± 0.3 dB for frequencies ranging from 300 to 3.0 GHz as presented in **Figure 7**. The active notch antenna output VSWR is better than 3:1 for frequencies from 0.5 to 3 GHz. All antennas presented in this paper can operate as passive and active antennas.

F-GHz	S11	S11°	S21	S21°
0.19	−31.76	0.964	24.13	158.9
0.279	0.93	−45.77	22.97	149.5
0.323	0.92	−53.39	22.45	145.3
0.413	0.89	−65.72	20.98	137.27
0.50	0.87	−77.1	19.54	130.3
0.59	0.83	−87.12	18.08	124.14
0.726	0.8	−100.8	16.22	115.7
0.816	0.77	−108.8	15.07	110.75
1.04	0.74	−126.2	12.74	100.13
1.21	0.71	−137.6	11.25	92.91
1.53	0.687	−154.2	9.29	82.06
1.75	0.67	−164.1	8.24	75.31
2.02	0.67	−174.6	7.27	67.82

Table 5.
LNA amplifier S parameters.

F-GHz	S12	S12°	S22	S22°
0.19	0.016	74.88	0.54	−22.98
0.279	0.021	65.77	0.51	−33.65
0.323	0.026	62.38	0.49	−39.2
0.413	0.03	57.9	0.46	−49.3
0.50	0.034	53.03	0.43	−57.5
0.59	0.038	48.18	0.40	−64.12
0.726	0.042	42.06	0.36	−74.86
0.816	0.044	39.53	0.34	−80.87
1.04	0.049	33.69	0.29	−94.96
1.21	0.051	30.05	0.26	−104
1.53	0.055	26.08	0.22	−119
1.75	0.058	23.14	0.20	−128.4
2.02	0.06	20.88	0.18	−138.8

Table 6.
LNA amplifier S parameters.

F-GHz	NFMIN	N11X	N11Y	Rn
0.4	0.070	0.3276	20.05	0.062
0.5	0.079	0.3284	24.56	0.056
0.7	0.112	0.334	36.08	0.050
0.9	0.144	0.3396	47.4	0.045
1	0.16	0.3424	52.98	0.042
1.9	0.306	0.3682	100.93	0.029
2	0.322	0.3711	106.01	0.029
2.4	0.387	0.3829	125.79	0.029
3	0.484	0.401	153.93	0.036
3.9	0.629	0.429	−167.3	0.059
5	0.808	0.4645	−125.53	0.11

Table 7.
LNA noise parameters.

5. New fractal active 0.4–3 GHz energy harvesting antenna

A compact notch antenna with fractal structure is shown in **Figure 8**. The antenna is printed on a 5580 Duroid substrate, 1.2 mm thick, with dielectric constant of 2.2. The notch antenna dimensions are 52.2 × 36.8 × 1.2 mm. The antenna center frequency is 1.7 GHz. The antenna bandwidth is around 100% for VSWR better than 3:1. The active notch antenna VSWR is better than 3:1 for frequencies from 0.4 to 3 GHz. The antenna beam width is around 82° at 1 GHz. An LNA is connected to the antenna feed line. The antenna is connected to the LNA via an input matching network. An output matching network connects the amplifier output port to a rectifying circuit. A compact DC network supplies the required voltages to the active antenna. The amplifier specification, S parameters, and the

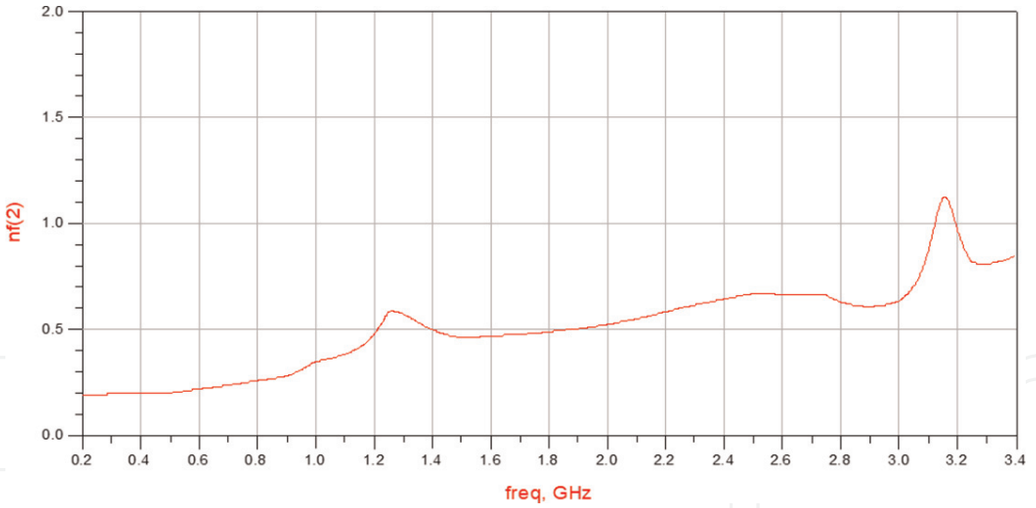

Figure 7.
Active notch antenna noise figure.

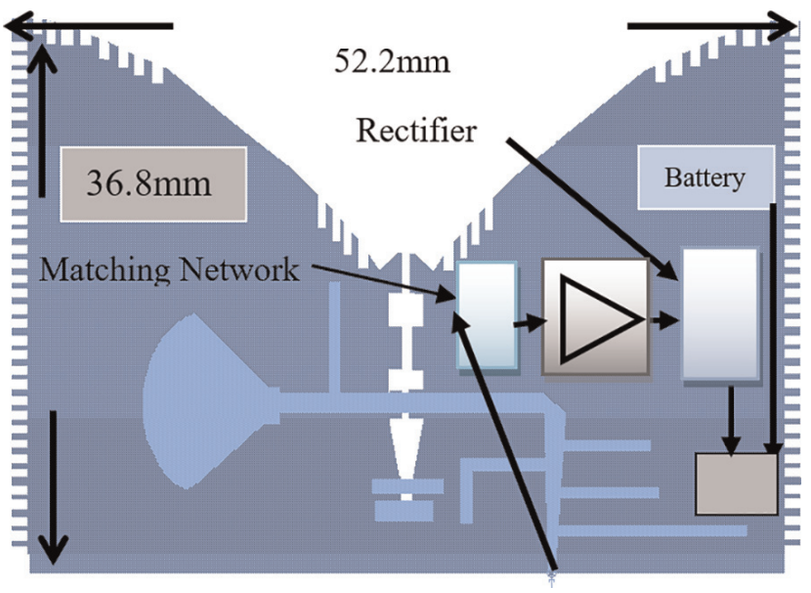

Figure 8.
A wideband fractal active notch antenna with fractal structure.

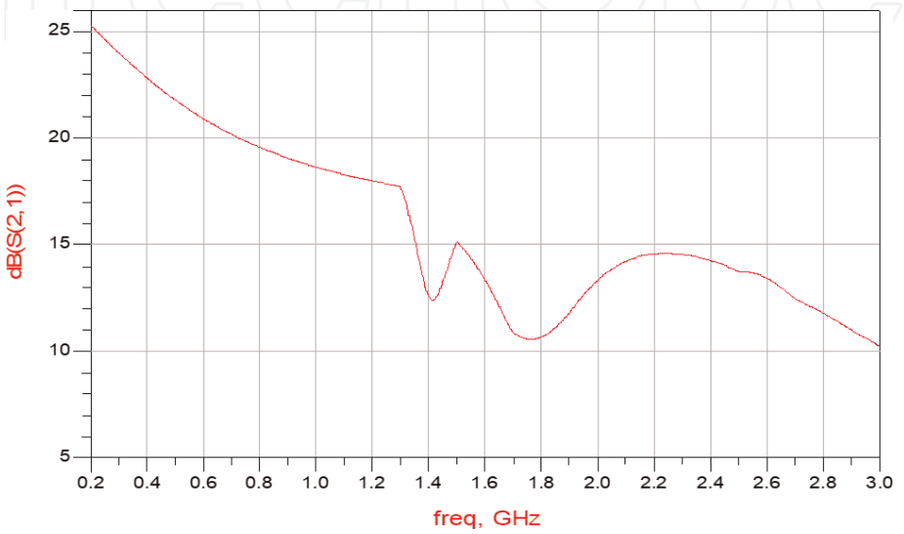

Figure 9.
A fractal active notch antenna S21 parameter.

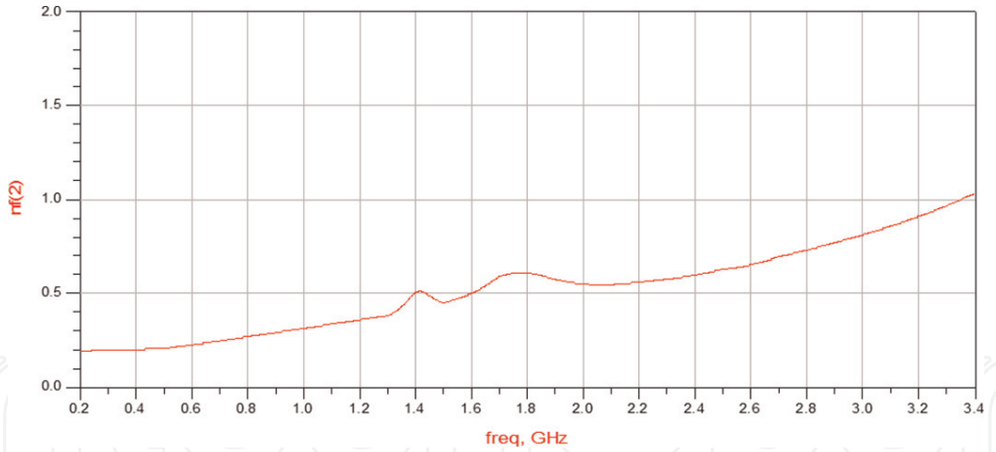

Figure 10.
Active fractal notch antenna noise figure.

amplifier noise parameters are listed in **Tables 4**–7. The active antenna gain is 21 ± 3 dB for frequencies from 400 MHz to 1.3 GHz, as presented in **Figure 9**. The active antenna gain is 12 ± 3 dB for frequencies from 1.3 to 3 GHz. The active notch antenna noise figure is 0.5 ± 0.3 dB for frequencies from 300 MHz to 3.0 GHz, as presented in **Figure 10**. The notch antenna output VSWR is better than 3:1 for frequencies from 0.5 to 3 GHz.

6. New wideband active 0.8–5.4 GHz energy harvesting slot antenna

A wideband T shape wearable slot antenna for energy harvesting applications is shown in **Figure 11**. The antenna electrical parameters were computed by using momentum software [38]. The volume of the T-shape slot antenna is 7 × 7 × 0.12 cm. The slot antenna center frequency is around 3 GHz. The computed S11 parameters

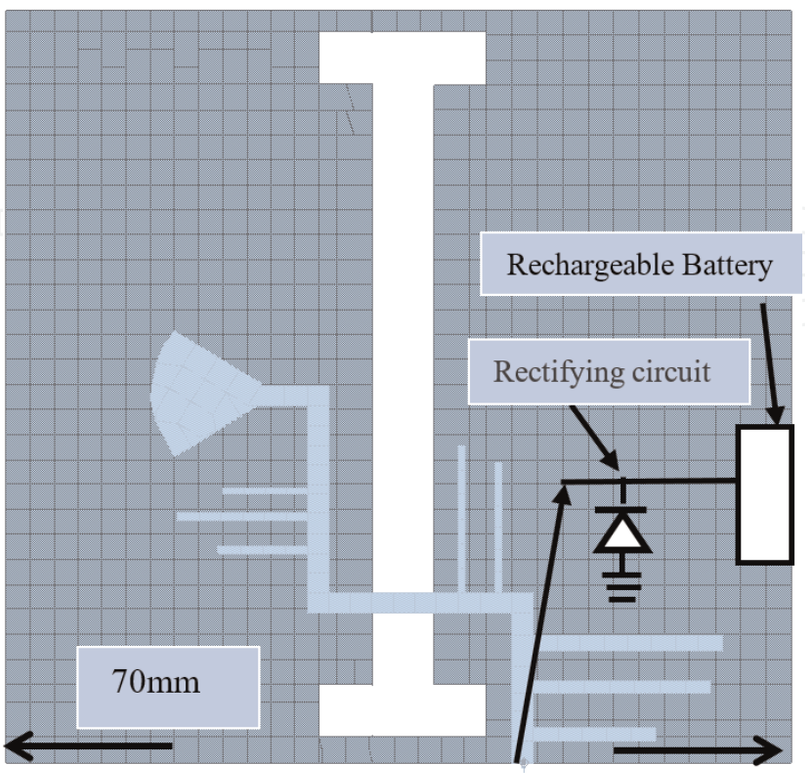

Figure 11.
A wideband energy harvesting slot antenna.

DOI: http://dx.doi.org/10.5772/intechopen.89699

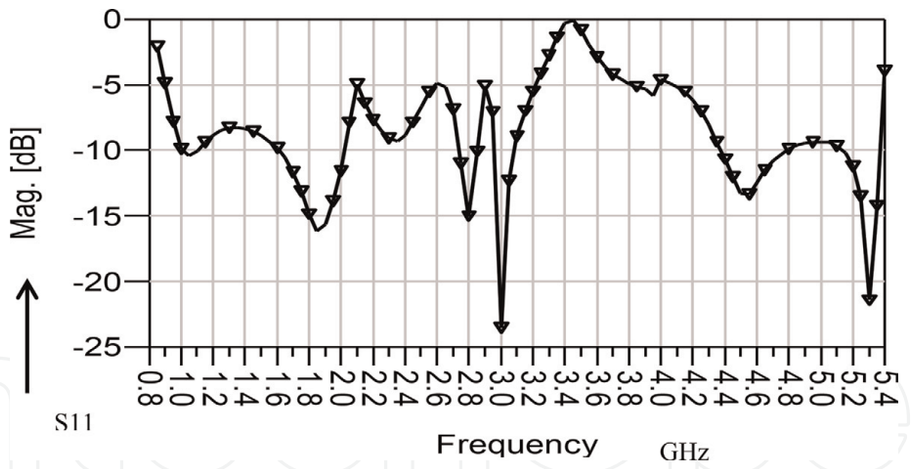

Figure 12.
Computed S11 of a wideband, 0.8–5.4 GHz, slot.

are presented in **Figure 12**. The antenna bandwidth is around 100% for VSWR better than 3:1. The antenna beamwidth is around 138° at 1 GHz as shown in **Figure 13**. The antenna gain is around 2.5 dBi. The antenna was designed also as an active antenna as shown in **Figure 14**. The slot antenna is connected to the LNA via an input matching network. The output matching network connects the amplifier output port to a rectifying circuit. For example, a MMIC LNA with 16 dB gain and 1 dB noise figure has DC power consumption of less than 18 mW in the frequency range from 70 MHz to 1 GHz. The system DC bias network supply the required voltages to the energy harvesting system. The amplifier specification is listed in **Table 5**. The amplifier complex S parameters are listed in **Tables 5** and **6**. The active slot antenna gain, S21 parameter, is presented in **Figure 15**. The active antenna gain is 23 ± 3 dB for frequencies from 200 to 900 MHz. The active antenna gain is 13 ± 3 dB for frequencies from 1 to 3 GHz. The active slot antenna noise

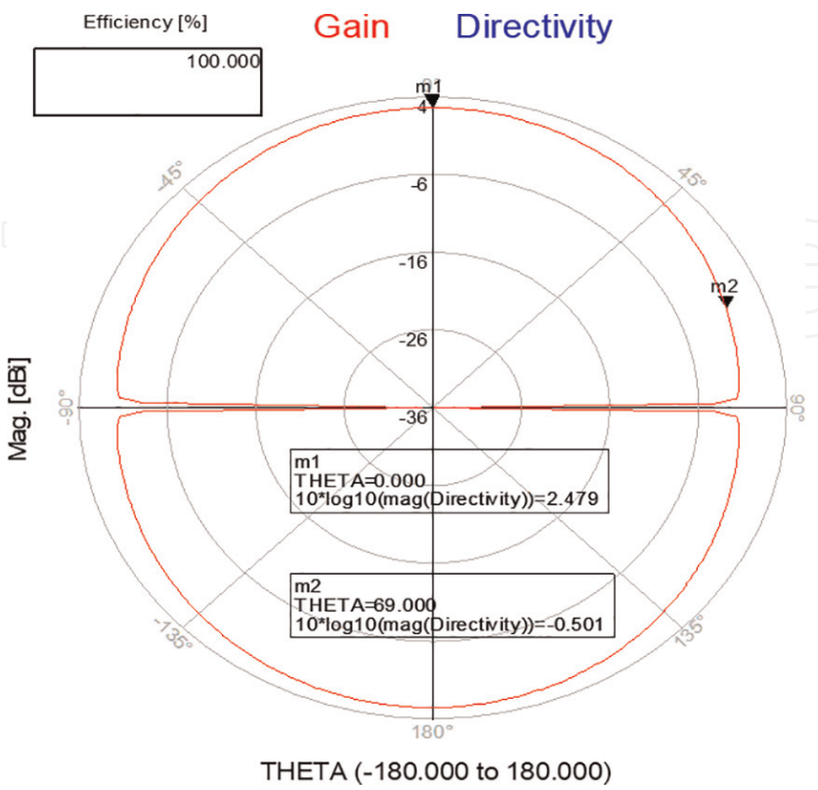

Figure 13.
Radiation pattern of the energy harvesting slot antenna.

figure is 0.5 ± 0.3 dB for frequencies from 200 MHz to 3.0 GHz. The computed S11 parameters of the T-shape slot on human body are presented in **Figure 16**. The dielectric constant of human body tissue was taken as 45. The antenna was attached to a shirt with dielectric constant of 2.21 mm thick.

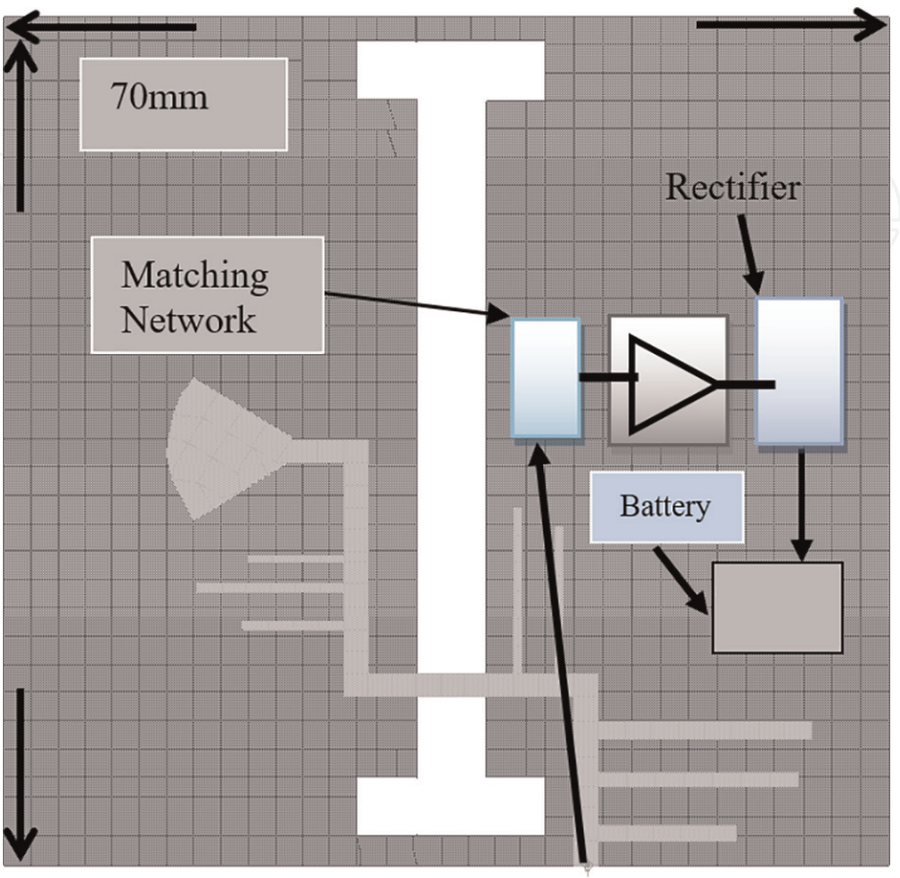

Figure 14.
A wideband active energy harvesting slot antenna.

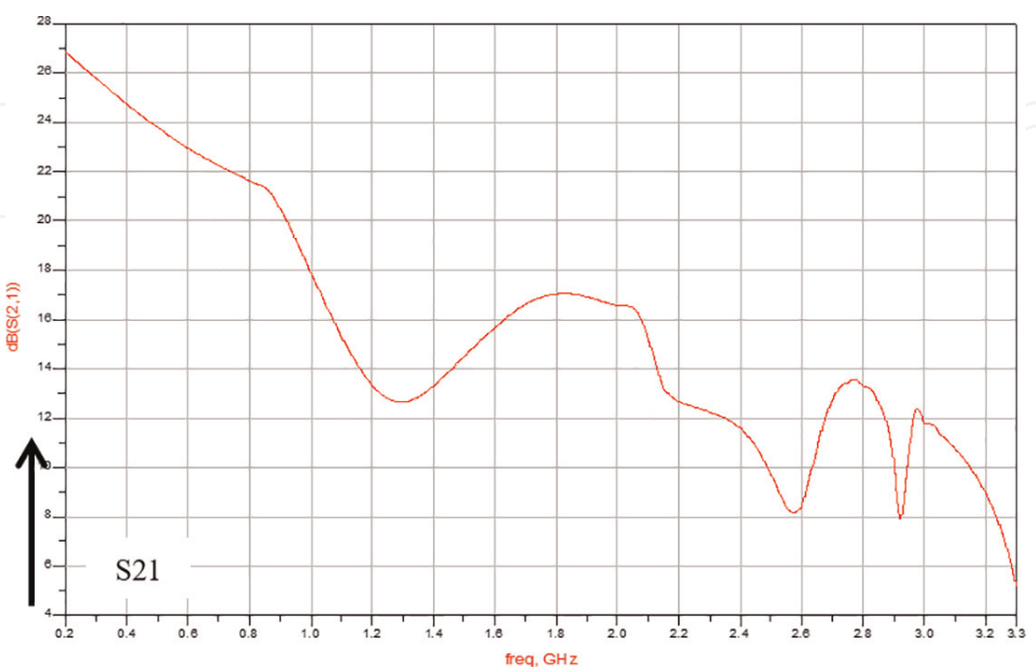

Figure 15.
Active energy harvesting slot antenna S21.

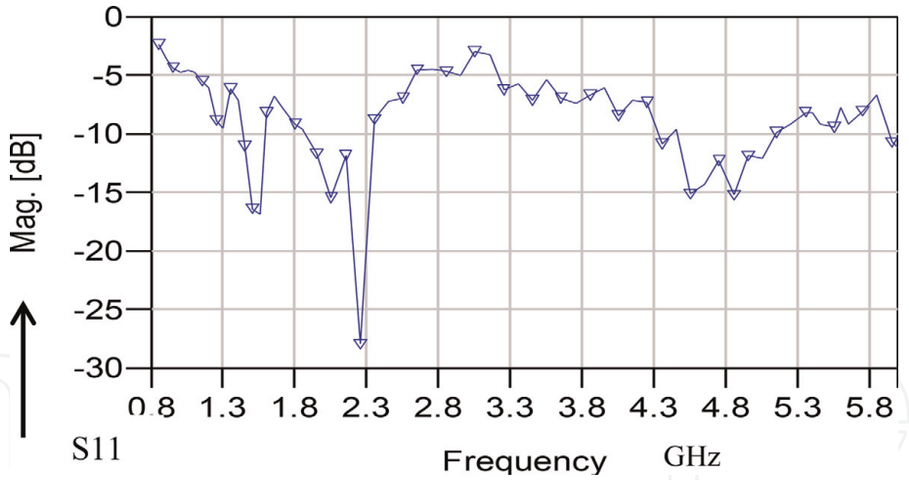

Figure 16.
Computed S11 of a wideband, 0.8–5.4 GHz, slot. Antenna on the human body.

7. Energy harvesting systems for medical and IOT applications

The notch and slot antennas' electrical performance near the human body was investigated by using the model shown in **Figure 17**. Properties of human body tissues are listed in **Table 8** [27, 28]. These properties were employed in the antenna design. Up to four energy harvesting antennas may be assembled in a belt and attached to the patient body as presented in **Figure 18**. The bias voltage to the active elements is supplied by a compact recorder battery. The DC cables from each harvesting antenna are connected to a rechargeable battery. The electromagnetic energy is converted to DC energy that may be employed to charge medical or commercial body area networks (BANs).

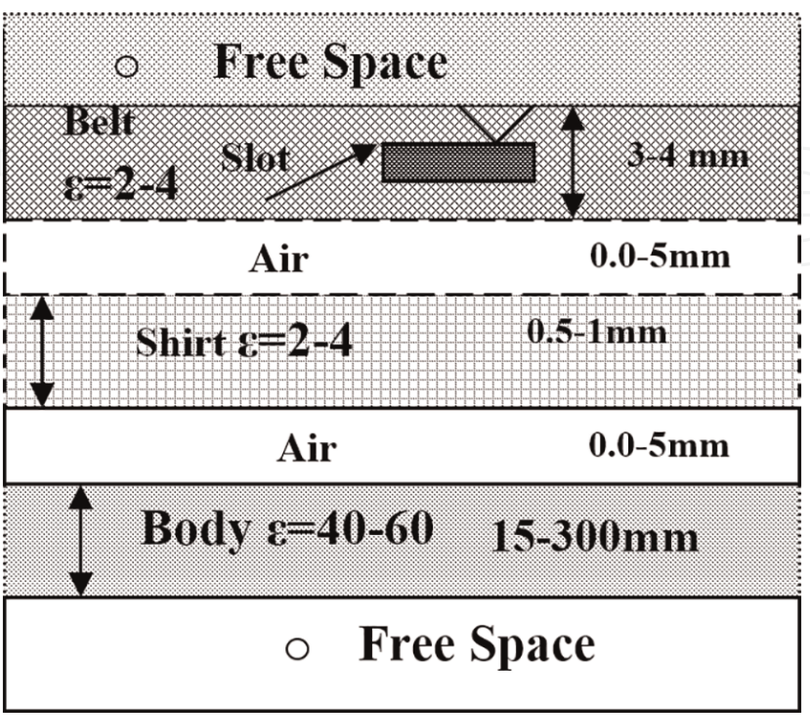

Figure 17.
Analyzed structure for wearable slot antennas.

Tissue	Property	600 MHz	1000 MHz
Fat	σ	0.05	0.06
	ε	5	4.52
Stomach	σ	0.73	0.97
	ε	41.41	39.06
Colon	σ	1.06	1.28
	ε	61.9	59.96
Lung	σ	0.27	0.27
	ε	38.4	38.4
Prostate	σ	0. 75	0.90
	ε	50.53	47.4
Kidney	σ	0.88	0.88
	ε	117.43	117.43

Table 8
Electrical properties of human body tissues.

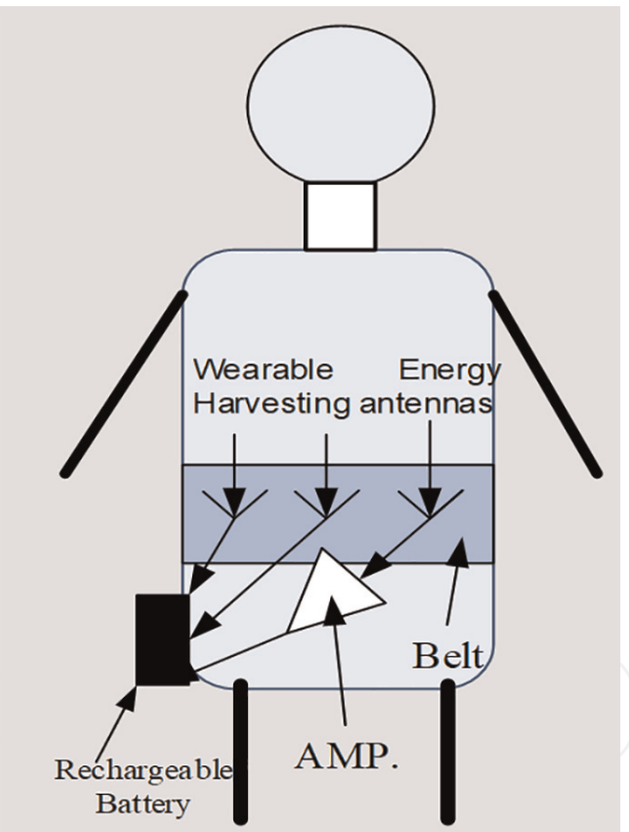

Figure 18.
Active wearable energy harvesting antennas.

8. Energy harvesting system

As presented in **Figure 1**, the energy harvesting system consists of an antenna, a rectifying circuit, and a rechargeable battery. A rectifier is a circuit that converts electromagnetic energy, alternating current AC, to direct current (DC). Half-wave rectifier or full wave rectifier may be used to convert electromagnetic AC energy to DC electrical energy. A half-wave rectifier is presented in **Figure 19**. A half-wave rectifier conducts only during the positive half cycle. It allows only one half of an AC waveform to pass through the load. The rectifier output DC voltage, V_{ODC}, is

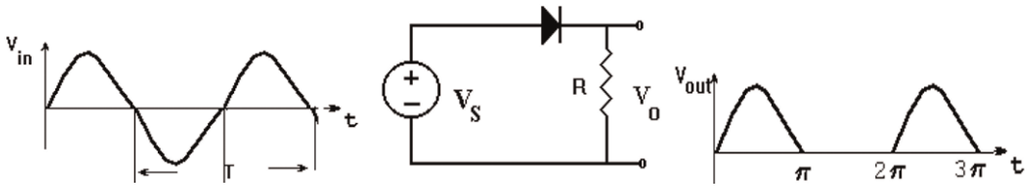

Figure 19.
Half-wave rectifier.

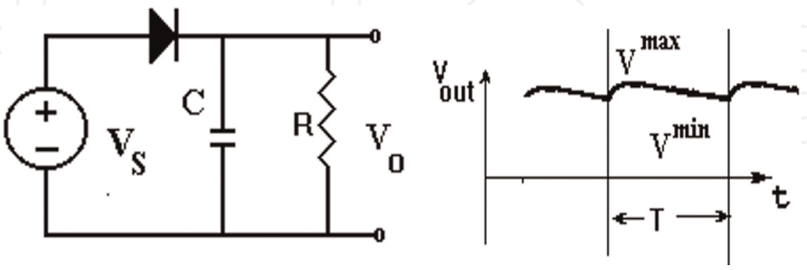

Figure 20.
Improved half-wave rectifier.

given in Eq. 5. The rectifier output voltage may be improved by connecting a capacitor in shunt to the resistor as presented in **Figure 20**.

$$\begin{aligned} V_{O,DC} &= \frac{1}{2\pi}\int_0^{2\pi} V_O^{MAX}\sin(\omega t)d(\omega t);\ \omega = 2\pi f \\ V_O &= V_S - V_{DON} \approx V_S;\ V_O^{MAX} = V_m \\ V_{ODC} &= V_m/\pi \end{aligned} \tag{5}$$

The improved half wave rectifier is shown in **Figure 20**.

$$Vripple = Vr = Vmax - Vmin = {}^{VDC}/_{fCR} \tag{6}$$

The time constant τ should be lower than T, where, $\tau = RC \ll T$. The half-wave rectifier efficiency is 40.6% as given in Eq. 7. Only 40.6% of the input AC power is converted into DC power. Where rf the diode resistance is negligible as compared to R.

$$\eta = \frac{\text{DC output power}}{\text{AC input power}} = \frac{\left(\frac{I_m}{\pi}\right)^2 R}{\left(\frac{I_m}{2}\right)^2 (R + rf)} \sim 0.406 \tag{7}$$

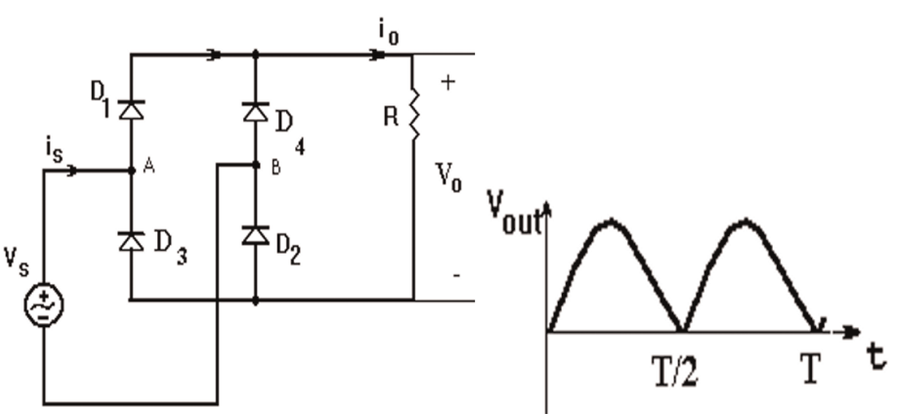

Figure 21.
Full-wave rectifier.

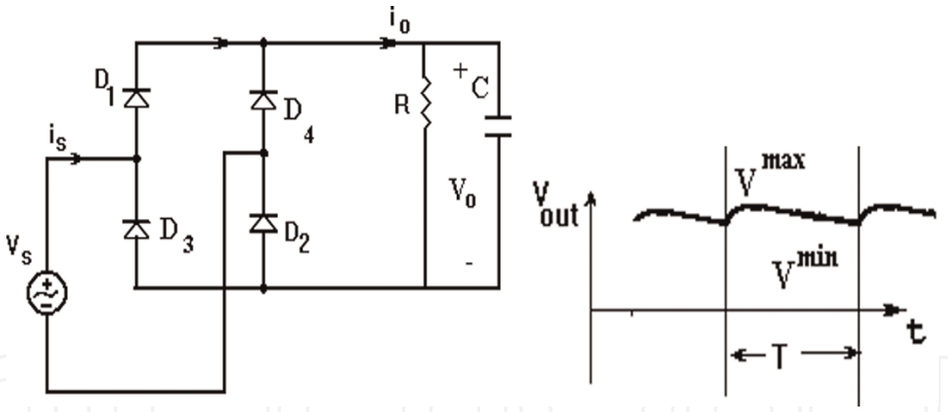

Figure 22.
Improved full-wave rectifier.

The bridge full-wave rectifier circuit is used usually for DC power supplies. It consists of four diodes, D1–D4, as shown in in **Figure 21**, connected to form a bridge. During the positive input half cycle, terminal A will be positive and terminal B will be negative. Diodes D1 and D2 will become forward biased and D3 and D4 will be reversed biased. The rectifier output DC voltage, $V_{ODC} = 2V_m/\pi$, may be improved by connecting a capacitor in the shunt to the resistor. The improved half-wave rectifier is presented in **Figure 22**.

The half-wave rectifier efficiency is 81.2% as presented in Eq. 8. This means that only 81.2% of the input AC power is converted into DC power.

$$\eta = \frac{\text{DC output power}}{\text{AC input power}} = \frac{\left(\frac{2I_m}{\pi}\right)^2 R}{\left(\frac{I_m}{2}\right)^2 (R + rf)} \sim 0.812 \tag{8}$$

A capacitor is used in the improved rectifier to get flat output voltage variation as function of time. The capacitor may be a voltage-controlled varactor diode. Varactors are voltage variable capacitors designed to provide electronic tuning of electrical devices. The output voltage ripple (see Eq. 6) of the improved rectifier may be tuned as function of the frequency of the received signal or of the load resistance R.

A Schottky diode may be used in the rectifier circuit. Schottky diodes are semiconductor diodes which has a low forward voltage drop and a very fast switching action. There is a small voltage drop across the diode terminals when current flows through the diode. The voltage drop of a Schottky diode is usually between 0.15 and 0.4 V. This lower voltage drop provides better system efficiency and higher switching speed. A normal diode has a voltage drop between 0.6 and 1.7 V. Electrical characteristics of Schottky diode and standard PN diodes are listed in **Table 9**. Typical I–V curves of commercial Schottky diodes are shown in **Figure 23**.

Parameter	Schottky diode	PN diode
Forward current mechanism	Majority carrier transport	Minority carrier transport
Reverse current	Less temperature dependence	Strong temperature dependence
Turn on voltage	Small—around 0.2 V	Comparatively large around 0.7 V
Switching speed	Fast	Limited

Table 9.
Electrical characteristics of Schottky diode and PN diodes.

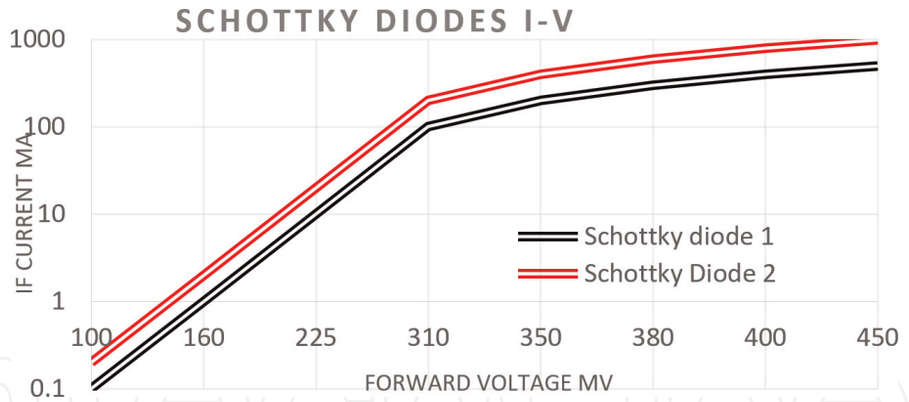

Figure 23.
Typical I–V curves of Schottky diodes.

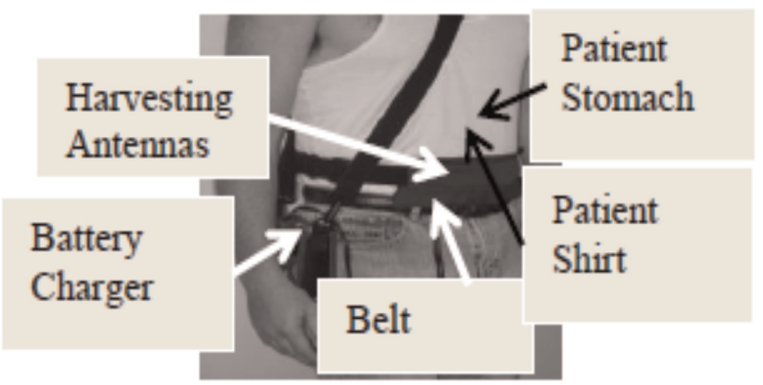

Figure 24.
Medical wearable harvesting system.

Figure 24 presents a wearable harvesting system and a wearable battery charger attached to the patient shirt.

9. Conclusion

This paper presents new ultra-wideband wearable passive and active energy harvesting systems and antennas in frequencies ranging from 0.4 to 8 GHz. The antennas are inserted in a belt and attached to the body. The antennas are compact and can be attached to the body. The antennas allow the patients' easy movement (running, jumping, and working).

The electromagnetic energy is converted to DC energy that may be employed to charge batteries, wearable medical devices, and commercial body area networks. The passive and active notch and slot antennas were analyzed by using 3D full-wave software. Harvested power from RF transmitting links is usually lower than 0.1 μW/cm^2. Active antennas may improve the energy harvesting system efficiency. All antennas presented in this paper can operate also as passive antennas. The active notch and slot antenna bandwidth are from 50 to 100% with VSWR better than 3:1. The slot antenna gain is around 3 dBi with efficiency higher than 90%. The antenna electrical parameters were computed near the human body. The active slot antenna gain is 24 ± 2.5 dB for frequencies ranging from 200 to 900 MHz. The active slot antenna gain is 13 ± 3dB for frequencies from 1 to 3.3 GHz. The active wearable antennas may be used in energy harvesting systems for wireless communication and medical applications. The RF energy harvesting system consists of an antenna, a

rectifying circuit, and a rechargeable battery. The harvesting energy system operates as a dual mode energy harvesting system. The low-noise amplifier is part of the receiving system. The LNA DC bias voltages are supplied by the receiving system.

Author details

Albert Sabban[1,2]

1 Kinneret Academic College, Israel

2 Ort Braude College, Karmiel, Israel

*Address all correspondence to: sabban@mx.kinneret.ac.il

References

[1] Paradiso JA, Starner T. Energy scavenging for mobile and wireless electronics. IEEE Pervasive Computing. 2005;**4**(1):18-27

[2] Valenta CR, Durgin GD. Harvesting wireless power: Survey of energy-harvester conversion efficiency in far-field, wireless power transfer systems. IEEE Microwave Magazine. 2014;**15**(4): 108-120

[3] Nintanavongsa P, Muncuk U, Lewis DR, Chowdhury KR. Design optimization and implementation for RF energy harvesting circuits. IEEE Journal on Emerging and Selected Topics in Circuits and Systems. 2012; **2**(1):24-33

[4] Devi KKA, Sadasivam S, Din NM, Chakrabarthy CK. Design of a 377 Ω patch antenna for ambient RF energy harvesting at downlink frequency of GSM 900. In: Proceedings of the 17th Asia Pacific Conference on Communications (APCC '11). Malaysia: Sabah; October 2011. pp. 492-495

[5] Rahim RA, Malek F, Anwar SFW, Hassan SLS, Junita MN, Hassan HF. A harmonic suppression circularly polarized patch antenna for an RF ambient energy harvesting system. In: Proceedings of the IEEE Conference on Clean Energy and Technology (CEAT '13). Malaysia: IEEE, Lankgkawi; November 2013. pp. 33-37

[6] Krakauskas M, Sabaawi AMA, Tsimenidis CC. Suspended patch microstrip antenna with cut rectangular slots for RF energy harvesting. In: Proceedings of the 10th Loughborough Antennas and Propagation Conference (LAPC '14). UK: Loughborough; November 2014. pp. 304-307

[7] Sabban A. Low Visibility Antennas for Communication Systems. USA: Taylor & Francis group; 2015

[8] Sabban A. Wideband RF Technologies and Antenna in Microwave Frequencies. USA: Wiley Sons; July 2016

[9] James JR, Hall PS, Wood C. Microstrip Antenna Theory and Design. London; 1981

[10] Sabban A, Gupta KC. Characterization of radiation loss from microstrip discontinuities using a multiport network modeling approach. IEEE Transactions on Microwave Theory and Techniques. April 1991; **39**(4):705-712

[11] Sabban A. A new wideband stacked microstrip antenna. In: IEEE Antenna and Propagation Symp., Houston, Texas, USA. June 1983

[12] Sabban A, Navon E. A MM-waves microstrip antenna array. In: I.E.E.E Symposium, Tel-Aviv. March 1983

[13] Balanis CA. Antenna Theory: Analysis and Design. 2nd ed. Wiley; 1996

[14] Sabban A. Multiport network model for evaluating radiation loss and coupling among discontinuities in microstrip circuits [PhD thesis]. University of Colorado at Boulder; January 1991

[15] Sabban A. Microstrip antenna arrays. U.S. Patent US 1986/4,623,893; 1986

[16] Sabban A. Wideband microstrip antenna arrays. I.E.E.E Antenna and Propagation Symposium MELCOM, Tel-Aviv; June 1981

[17] Fujimoto K, James JR, editors. Mobile Antenna Systems Handbook. Boston, USA: Artech House; 1994

[18] Sabban A. New wideband notch antennas for communication systems.

Wireless Engineering and Technology Journal. April 2016:75-82

[19] Sabban A. Dual polarized dipole wearable antenna. U.S Patent number: 8203497. USA, June 19, 2012

[20] Sabban A. Wideband tunable printed antennas for medical applications. In: IEEE Antenna and Propagation Symp., Chicago, IL, USA. 2012, July 2012

[21] Sabban A. New wideband printed antennas for medical applications. I.E.E. E Transactions on Antennas and Propagation, January. 2013;**61**(1):84-91

[22] Sabban A. Comprehensive study of printed antennas on human body for medical applications. International Journal of Advance in Medical Science (AMS). February 2013;**1**:1-10

[23] Kastner R, Heyman E, Sabban A. Spectral domain iterative analysis of single and double-layered microstrip antennas using the conjugate gradient algorithm. I.E.E.E Transactions on Antennas and Propagation. Sept. 1988; **36**(9):1204-1212

[24] Sabban A. Microstrip antenna arrays. In: Nasimuddin N, editor. Microstrip Antennas. InTech; 2011. pp. 361-384. Available at: http://www.intechopen.com/articles/show/title/microstrip-antenna-arrays. ISBN: 978-953-307-247-0

[25] Sabban A. New wideband wearable notch antenna for energy harvesting applications. In: 12th European Conference on Antennas and Propagation EuCAP 2018, United Kingdom. 2018

[26] Chirwa LC, Hammond PA, Roy S, Cumming DRS. Electromagnetic radiation from ingested sources in the human intestine between 150 MHz and 1.2 GHz. IEEE Transaction on Biomedical Engineering. April 2003; **50**(4):484-492

[27] Werber D, Schwentner A, Biebl EM. Investigation of RF transmission properties of human tissues. Advances in Radio Science. 2006;**4**:357-360

[28] Gupta B, Sankaralingam S, Dhar S. Development of wearable and implantable antennas in the last decade. In: Microwave Symposium (MMS), 2010 Mediterranean. 2010. pp. 251-267

[29] Thalmann T, Popovic Z, Notaros BM, Mosig JR. Investigation and design of a multi-band wearable antenna. In: 3rd European Conference on Antennas and Propagation, EuCAP. 2009. pp. 462-465

[30] Salonen P, Rahmat-Samii Y, Kivikoski M. Wearable antennas in the vicinity of human body. In: IEEE Antennas and Propagation Society International Symposium. Vol. 1. 2004. pp. 467-470

[31] Kellomaki T, Heikkinen J, Kivikoski M. Wearable antennas for FM reception. In: First European Conference on Antennas and Propagation, EuCAP. 2006. pp. 1-6

[32] Sabban A. Wideband printed antennas for medical applications. In: APMC 2009 Conference, Singapore. Dec. 2009

[33] Alomainy A, Sani A, et al. Transient characteristics of wearable antennas and radio propagation channels for ultrawideband body-centric wireless communication. IEEE Transactions on Antennas and Propagation. April 2009; **57**(4):875-884

[34] Klemm M, Troester G. Textile UWB antenna for wireless body area networks. I.E.E.E. Transactions on Antennas and Propagation. Nov. 2006; **54**(11):3192-3197

[35] Izdebski PM, Rajagoplan H, Rahmat-Sami Y. Conformal ingestible capsule antenna: A novel chandelier meandered design. IEEE Transactions on Antennas and Propagation. April 2009;**57**(4):900-909

[36] ADS software. Agilent. Available at: http://www.home.agilent.com/agilent/product.jspx?cc=IL&lc=eng&ckey=1297113&nid=34346.0.00&id=1297113